European Journal of Radiology 114 (2019) 38–44

Contents lists available at ScienceDirect

European Journal of Radiology

journal homepage: www.elsevier.com/locate/ejrad

Research article

Using biparametric MRI radiomics signature to differentiate between benign and malignant prostate lesions

Min Xu[a,b,1], Mengjie Fang[b,c,1], Jian Zou[e], Shudong Yang[f], Dongdong Yu[b,c], Lianzhen Zhong[b,c], Chaoen Hu[b,c], Yali Zang[b,c], Di Dong[b,c,d,**], Jie Tian[b,c,d,**], Xiangming Fang[a,*]

[a] Imaging Center, Wuxi People's Hospital, Nanjing Medical University, No. 299, Qingyang Road, Liangxi District, Wuxi, Jiangsu Province, 214023, China
[b] CAS Key Laboratory of Molecular Imaging, Institute of Automation, Chinese Academy of Sciences, Beijing 100190, China
[c] University of Chinese Academy of Sciences, Beijing, 100190, China
[d] Beijing Key Laboratory of Molecular Imaging, Beijing 100190, China
[e] Center of Clinical Research, Wuxi People's Hospital, Nanjing Medical University, No. 299, Qingyang Road, Liangxi District, Wuxi, Jiangsu Province, 214023, China
[f] Department of Pathology, Wuxi People's Hospital, Nanjing Medical University, No. 299, Qingyang Road, Liangxi District, Wuxi, Jiangsu Province, 214023, China

ARTICLE INFO

Keywords:
Prostate cancer
Radiomics
Biparametric magnetic resonance imaging
Medical imaging

ABSTRACT

Purpose: To investigate the efficiency of radiomics signature in discriminating between benign and malignant prostate lesions with similar biparametric magnetic resonance imaging (bp-MRI) findings.

Experimental design: Our study consisted of 331 patients underwent bp-MRI before pathological examination from January 2013 to November 2016. Radiomics features were extracted from peripheral zone (PZ), transition zone (TZ), and lesion areas segmented on images obtained by T2-weighted imaging (T2WI), diffusion-weighted imaging (DWI), and its derivative apparent-diffusion coefficient (ADC) imaging. The individual prediction model, built using the clinical data and biparametric MRI features (Bp signature), was prepared using data of 232 patients and validated using data of 99 patients. The predictive performance was calculated and demonstrated using receiver operating characteristic (ROC) curves, calibration curves, and decision curves.

Results: The Bp signature, based on the six selected radiomics features of bp-MRI, showed better discrimination in the validation cohort (area under the curve [AUC], 0.92) than on each subcategory images (AUC, 0.81 on T2WI; AUC, 0.77 on DWI; AUC, 0.89 on ADC). The differential diagnostic efficiency was poorer with the clinical model (AUC, 0.73), built using the selected independent clinical risk factors with statistical significance ($P < 0.05$), than with the Bp signature. Discrimination efficiency improved when including the Bp signature and clinical factors [i.e., the individual prediction model (AUC, 0.93)].

Conclusion: The Bp signature, based on bp-MRI, performed better than each single imaging modality. The individual prediction model including the radiomics signatures and clinical factors showed better preoperative diagnostic performance, which could contribute to clinical individualized treatment.

1. Introduction

Prostate cancer (PCa) is the most common cause of new cases of cancer, and is the third leading cause of estimated deaths among male individuals, according to cancer statistics estimated by the American Cancer Society [1]. Among the 10 most common cancers in men in China, prostate cancer has a marked upward trend in age-standardized mortality rates. For prostate cancer patients, radical prostatectomy is appropriate for any patient whose cancer appears clinically localized to the prostate according to NCCN 2018. Treatment of non-prostate cancer patients are usually transurethral resection of the prostate (TURP), antiandrogenic therapy, anti-inflammatory therapy and so on, which depends on specific prostate diseases. A good prognosis can be obtained with accurate diagnosis and immediate treatment [2].

Conventional diagnostic methods for prostate cancer are prostate-specific antigen (PSA) level, digital rectal examination (DRE), and biparametric magnetic resonance imaging (bp-MRI) [3]. The combination of PSA screening and digital rectal examination, which can detect PCa

* Corresponding author at: Imaging Center, Wuxi People's Hospital, Nanjing Medical University, No. 299, Qingyang Road, Liangxi District, Wuxi, Jiangsu Province, 214023, China.
** Corresponding authors at: CAS Key Laboratory of Molecular Imaging, Institute of Automation, Chinese Academy of Sciences, Beijing, 100190, China.
E-mail addresses: di.dong@ia.ac.cn (D. Dong), jie.tian@ia.ac.cn (J. Tian), xiangming_fang@njmu.edu.cn (X. Fang).
[1] Contributed equally to this work.

https://doi.org/10.1016/j.ejrad.2019.02.032
Received 23 November 2018; Received in revised form 19 February 2019; Accepted 23 February 2019

at an early stage, is widely used in the PCa general examination in clinical practice [4]. As a tumor marker, the PSA level has high sensitivity but low specificity, benign prostate conditions also affect PSA levels [5,6]. A pathologic examination used to be the ground truth in discriminating between benign and malignant tumors. Approximately over thirty percent of men who have experienced prostate biopsy occur pain, infection, fever, haematuria, transient dysuria and about 1% require to be hospitalized for observation [7].

In past decades, bp-MRI has gradually become a crucial assessment tool in staging and newly diagnosed PCa [8]. Patients with a raised PSA level are usually requested to have a pelvic MRI scan before prostate biopsy on clinical practice [9]. According to the Prostate Imaging Reporting and Data System (PI-RADS) (version 2), T2-weighted imaging (T2WI), diffusion-weighted imaging (DWI), and its derivative apparent-diffusion coefficient (ADC) maps have a leading role in prostate cancer diagnosis [10]. Anatomic information and TNM staging is primarily provided by T2WI, whereas functional and physiologic information is provided by DWI and ADC [11,12]. Many patients have similar imaging findings for benign and malignant prostate lesions, which is difficult to differentiate these lesions.

The emerging technique radiomics is a noninvasive, efficient, and reliable method used in disease diagnosis and prediction [13,14]. In previous research, radiomics has been mostly applied in oncology such as colorectal cancer, lung cancer, and breast cancer [15–17]. Experimental results showed that radiomics connected imaging features with clinical manifestations and features at the molecular gene level. This combination can attain better recognition rates in tumor classification, tumor metastasis, and recurrence [18–20]. In addition, radiomics has also made significant progress toward application maturity in different medical image modalities such as ultrasonic imaging, computed tomography (CT), MRI and positron emission tomography (PET) [15,16,21].

Therefore, our study aims to (1) investigate whether radiomics signatures based on bp-MRI can help to improve the discrimination efficiency of prostate cancer, and (2) develop and validate an individualized prostate cancer prediction model that incorporates clinical independent risk factors and radiomics signatures.

2. Methods

2.1. Patients

The primary cohort of our study consisted of an existing database of 331 inpatients who underwent pathological examination and pre-operative bp-MRI between the dates of January 2013 (initiation of prostate bp-MRI program at our institution) and November 2016. The entire MRI records of the included patients were obtained from the Picture Archiving and Communication System (PACS) of our hospital. Ethical approval was obtained for this retrospective study, and the informed consent requirement of patients was waived.

Patients included in our study followed the inclusion criteria as (1) prostate lesions with definite boundaries on three types of MR images according to PI-RADS version 2 (T2WI, DWI, and ADC) (Fig. 1); (2) preoperative pathological examination results; (3) PZ, TZ, and lesion areas all could be segmented on the MR images (considering of PZ areas of patients with severe prostate hyperplasia were hard to segment); and (4) complete clinical information.

The Exclusion criteria were (1) patients who had definite extra-prostatic extension/invasive behavior; (2) patients who had a time interval between screening and pathological examination of more than 2 months.

Among the identified 331 patients in the study cohort (range, 46–94 years; mean age, 71 years), pathological examination revealed 166 patients had PCa. The primary cohort consisted of 232 patients who were treated from January 2013 to October 2015. A total of 99 patients from November 2015 to November 2016 constituted the independent validation cohort. The primary cohort and validation cohort were divided by chronological order.

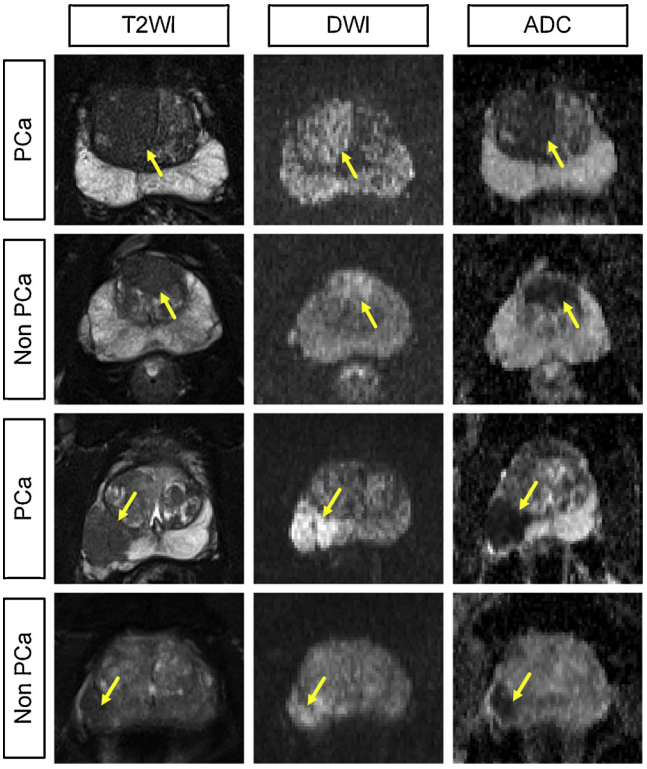

Fig. 1. Axial images of predicted samples in bi-parametric MR images and the four patients had different pathological results.

We collected the clinical details from our electronic hospital information system, which included the PSA levels, carcinoembryonic antigen (CEA) level, cancer antigen-125 (CA125) level, cancer antigen-19-9 (CA19-9) level, diabetes, and hypertension conditions. The cutoff values for PSA level were 10 ng/mL. The threshold value for the CA125 level and CA 19-9 level was 35 U/mL, whereas that of the CEA level was 5 μg/L, based on the normal range used in our hospital.

2.2. Magnetic resonance imaging protocols

All patients were scanned at a single institution with 3.0-T MR scanners (MAGNETOM Verio, Siemens Healthcare, Erlangen, Germany) using pelvic phased-array coils. To guarantee the image quality, the MR machine was checked on by a hospital radiological technician every month and was further maintained by a Siemens engineer on a bi-monthly basis. For every standard prostatic MRI examination conducted in our hospital, the protocol included a combination of T1-weighted imaging (T1WI), T2WI, DWI and its derivative ADC imaging. We used three types of MR images in our study: T2WI, DWI, and ADC. The parameters for the axial, coronal, and sagittal T2WI were repetition time/echo time (TR/TE), 4000/100 ms; section thickness, 3 mm; flip angle, 150°; intersection gap, 3 mm; pixel spacing, 0.75/0.75; field of view (FOV), 216 mm^2 × 240 mm^2 and matrix, 288 × 320. The parameters of the used readout segmentation of long variable echo-trains (RESOLVE) DWI were the used b values, 0 s/mm^2, 800 s/mm^2; TR/TE, 3200/84 ms; section thickness, 3 mm; flip angle, 90°; intersection gap, 3 mm; FOV, 250 mm^2 × 250 mm^2; matrix, 192 × 192).

2.3. Segmentation

The standard of histological-radiological correlations was established through a systematic consensus-seeking correlative review of histological and MR findings by an experienced genitourinary

pathologist. Anatomical landmarks including prostatic capsule, urethra and ejaculatory ducts were used to pinpoint the appropriate region of interest (ROI), for example, the transition zone was defined as tissue around the urethra separated from the peripheral zone by'surgical capsule' delineated as a low signal line on T2W-MRI [10].

Potentially clinically significant tumor foci within each RP specimen were identified. For patients with multiple significant lesions, lesions > 0.5 mL in size [22–24] were all determined for each prostate section for further analysis. Lesions, PZ and TZ were confirmed and segmented on both the T2WI, DWI and ADC MR images. The segmentation section was selected, based on the largest lesion layer of benign and malignant lesions. The areas were segmented by using a free, open-source multiplatform image analysis software application for visualization and medical image computing (ITK SNAP version 3.6.0; available at: http://www.itksnap.org/).

The three areas were all manually drawn by a radiologist with 3 years of experience (i.e., Reader 1). Integrated imaging data of 40 patients treated from January 2013 to November 2016 were selected randomly from the study cohort, intraobserver segmentation was performed by Reader 1 three months later, and interobserver segmentation reproducibility was performed by another radiologist with 30^{+} years of prostatic MRI interpretation experience (i.e., Reader 2). During the segmentation process, the doctors were blinded to the histologic results and all clinical information of the retrospective prostate MR images.

2.4. Radiomics feature extraction

On each MR image, 324 radiomics features were extracted from each area, (i.e., the PZ area, the TZ area, and the lesion area). Therefore, the overall number of the radiomics features in this study was 2916.

For each area on each MR image, the value of the area (i.e., area-based feature [n = 1]) and features that were based on the original grayscale histogram (i.e., histogram-based feature [n = 23]) were first extracted. Three types of image filtering processes (i.e., gradient filtering, standard deviation filtering, and average filtering) were implemented on the original images. Based on the three filtered images and one nonfiltered image, the following features were extracted: features based on Gray Level Co-occurrence Matrix (GLCM-based features [n = 23]), features based on Gray Level Run Length Matrix (i.e., GLRLM-based features [n = 11]), features based on Gray Level Size Zone Matrix (i.e., GLSZM-based features [n = 13]), features based on Neighborhood Gray Tone Difference Matrix (i.e., NGTDM-based features [n = 5]), and features based on normalized grayscale histogram (i.e., norm-histogram-based features [n = 23]).

The characteristics of the first order texture were quantified by using histogram-based features and norm-histogram-based features. The characteristics of the second order texture were quantified by using GLCM-based features. The characteristics of the high order texture were quantified by using GLRLM-based features, GLSZM-based features, and NGTDM-based features.

2.5. Feature selection and model building

Feature selection and radiomics signature building were conducted on the basis of primary cohort. The intra- and inter observer agreement of feature extraction were evaluated through intraclass correlation coefficients (ICCs). An ICC greater than 0.8 indicated good agreement [25]. Stable and reproducible features were selected.

Features with a Pearson correlation coefficient > 0.75 were then grouped as a category [26]. To remove redundant features, only features with the highest relief F score among the categories were entered into the signature building process [27].

Four radiomics signatures (i.e. T2WI signature, DWI signature, ADC signature and Bp signature) were respectively built, based on the features of each single imaging modality and a combination of multiple modalities. To select the most powerful predictive combination of features, we use the least absolute shrinkage and selection operator (LASSO) regularization method in 1000 bootstrap resamples, which is proved effective for high-dimensional medical data clinically [15]. The logistic regression model was used to build each radiomics signature.

To simulate the usual clinical decision, multivariable logistic regression analysis incorporated the clinical factors (i.e., age, PSA level, CEA level, CA125 level, CA19-9 level, hypertension, and diabetes) to build a clinical model. Backward step-wise variable selection was applied to clinical model building with the Akaike information criterion (AIC) as the stopping rule [28]. Using the same modeling method, a quantitative and easy-to-use individual prediction model was built to predict individual PCa probability, based on the Bp signature and the clinical independent risk factors.

2.6. Statistical analysis

Univariate analysis was applied to assess the relationship between the characteristics of the patients and prostate disease type. To identify the potential association of variables with the prostate cancer, we assessed continuous variables by using the independent *t*-test or the Mann–Whitney *U* test, and evaluated categorical variables by using the chi-square test or the Fisher exact test. Multivariable logistic regression analysis was used to identify the independent predictors in the combination of features. The odds ratio was used to indicate the degree of risk when the classification result was "1." The ROC curves and AUCs of the predictors were obtained to assess their predictive performance and were compared using the Delong test. The point on ROC curve in the primary cohort for which the positive likelihood ratio was maximal was seen as the optimal cutoff threshold value and was applied to the validation cohort. The accuracy of the predictor was assessed using the values of sensitivity and specificity.

The calibration efficiency of Bp signature was intuitively demonstrated on calibration curve accompanied by Hosmer–Lemeshow test. The clinical value of individual prediction model was assessed by decision curve analysis, which quantified the net benefits at different threshold probabilities in the two cohorts [29]. With the concern that there may be confounding within the derived results, we conducted a stratified analysis by age and PSA level.

3. Results

3.1. Clinical characteristics of the patients

There were no significant differences in clinical characteristics and pathological results between the two cohorts (Table 1), which confirmed their use as the primary and validation cohorts. Patients with PCa constituted 49.1% and 52.5% of the primary and validation cohorts respectively.

In addition, between the PCa patients group and non-PCa patients group, there were no significant differences in the primary and validation cohorts in the levels of CEA, CA125, and CA19-9, or in the presence of diabetes and hypertension ($P > 0.05$; Table 2). Age and the proportion of abnormal PSA findings were significantly higher in PCa patients than non-PCa patients in both cohorts.

3.2. Radiomics signature and clinical model building

Many radiomics features (461 T2WI features, 211 ADC features, and 216 DWI features) showed satisfactory inter- and intraobserver agreement (i.e., the ICCs were > 0.8). After removing the highly correlated features, four radiomics signatures were built using the LASSO method. This information is presented in the Supplementary Material. It should be noted that, among the features analyzed from the 331 patients, 2916 features were finally reduced to two predictors from the DWI sequence and to four predictors from the corresponding ADC image, which

Table 1
Clinical characteristics of patients in the primary cohort and validation cohort.

Characteristics	Primary cohort		P	Validation cohort		P
	Non-PCa	PCa		Non-PCa	PCa	
No. of patients	118	114		47	52	
Age (y)			0.00012			0.0032
< 65	33	12		16	7	
65–75	58	59		26	26	
> 75	27	43		5	19	
PSA			< 0.0001			< 0.0001
< 10 ng/mL	57	17		26	8	
> 10 ng/mL	61	97		21	44	
CEA			0.0657			0.5826
< 5 μg/L	115	105		43	50	
> 5 μg/L	3	9		4	2	
CA125			1			NA
< 35 U/mL	117	113		47	52	
> 35 U/mL	1	1		0	0	
CA19-9			0.1379			1
< 35 U/mL	107	109		45	49	
> 35 U/mL	11	5		2	3	
Diabetes			0.4149			0.5127
0	100	92		36	38	
1	18	22		10	14	
Hypertension			0.0578			0.8996
0	58	41		22	25	
1	60	73		25	27	

Table 2
Clinical factors in the primary and validation cohorts.

Characteristic	Primary cohort	Validation cohort	P
Age, y (mean ± SD)	71.13 ± 7.72	70.08 ± 7.81	0.2634
PSA			0.6638
< 10 ng/mL	74	34	
> 10 ng/mL	158	65	
CEA			0.7442
< 5 μg/L	220	93	
> 5 μg/L	12	6	
Pathology			0.5725
Benign	118	47	
Malignant	114	52	

SD, standard deviation.

constructed the Bp signature.

For clinical model building, backward step-wise selection showed that age and PSA were important independent indicators. The corresponding regression equation is listed in the Supplementary Material.

3.3. Predictive performance of the radiomics signatures

Receiver operating curves were used to compare using single MR image type and biparametric MR images to discriminate between patients with and without PCa. For PCa prediction, T2WI, ADC imaging, and DWI yielded AUCs of 0.812, 0.893, and 0.775, respectively. The ROC curves in Fig. 2(A) and (B) indicated that the Bp signature showed better discrimination efficiency, and that the AUC further improved to 0.920. The Delong test revealed significant differences between the AUCs of the Bp signature and each signal MR image type (T2WI: P = 0.009; ADC: P = 0.048; and DWI: P = 0.001). The Bp signature also yielded not only the highest sensitivity (0.873, 0.827 respectively), but also highest specificity (0.839, 0.894 respectively) in discriminating between lesions in the primary and the validation cohorts (Appendix Table S1).

3.4. Development of an individual prediction model

The Bp signature, age, PSA level, CEA level, and hypertension appeared to be useful for discriminating between malignant and benign prostate lesions in the primary cohort (P < 0.1). These variables were subjected to multivariable logistic regression analysis. The Bp signature, age, and PSA level were independent predictors (Table 3). An individual prediction model was then built, based on the three variables with their regression coefficients, and was presented as the nomogram (Appendix Fig. S1). The ROC curves in Fig. 2(C) and (D) indicated that the individual prediction model had the best discrimination efficiency, and that the AUC improved to 0.933 (Appendix Table S2).

3.5. Validation of the individual prediction model

The validation cohort indicated good calibration in differentiating between benign and malignant lesions (Fig. 3(A) and (B)). The Hosmer–Lemeshow test yielded a nonsignificant statistic (P = 0.586 and P = 0.201 in the primary cohort and validation cohort, respectively), which suggested no departure from a perfect fit. The AUC of the individual prediction model for discrimination was 0.933. Furthermore, the stratified analysis showed the individual prediction model was still significant after adjusting for sex and PSA level (Appendix Fig. S2).

3.6. Clinical use

The prediction efficiency of the individual prediction model for PCa is presented by the decision curve analysis in Fig. 4. The decision curve showed that, compared to the treat-all-patients scheme or the treat-none scheme, using our individual prediction model to identify PCa and non-PCa patients added more benefit if the threshold probability of a patient or doctor was > 10%.

The prediction efficiency of the individual prediction model for PCa is presented by the decision curve analysis in Fig. 4. The decision curve showed that, compared to the treat-all-patients scheme or the treat-none scheme, using our individual prediction model to identify PCa and non-PCa patients added more benefit if the threshold probability of a patient or doctor was > 10%. Undiagnosed prostate cancer patients will miss the best time for treatment, which results in poor prognosis. And for the non-prostate cancer patients, the overtreatment is harmful. With a good prediction accuracy, our model is able to benefit patients care without subjecting them to unnecessary interventions and thus could be very helpful for clinical management.

4. Discussion

In our research, we developed a noninvasive individual prediction model to differentiate prostate lesions with clear boundaries in a primary cohort, and assessed its performance on an independent validation set. Based on the primary cohort, an individual prediction model incorporating significant clinical risk factors and Bp signature was constructed with the goal of transferring this model into an easy-to-use tool.

Six potential predictors constructed the Bp signature, which were reduced from 126 candidate radiomics features extracted from multiple areas and bp-MRI by examining the predictor-outcome association by shrinking the regression coefficients with the LASSO method. Combining multiple imaging features, Bp signature demonstrated favorable discrimination efficiency in the primary cohort (AUC, 0.887), and improved in the validation cohort (AUC, 0.920). Improved discrimination efficiency indicated that the radiomics signature was stable and robust for PCa prediction, which implied its universality.

Previous studies have revealed that age and the PSA level are correlated with prostate diseases [3,4]. According to the NCCN Clinical Practice Guidelines in Oncology for Prostate Cancer [30], a PSA level > 10 ng/mL, Gleason score of 9 or 10, and clinical stage T2b or higher were assumed to be adverse prognostic factors. Hence, our study set 10 as the threshold value of PSA to determine its efficiency in prostate cancer discrimination. Except for age and PSA, our study also

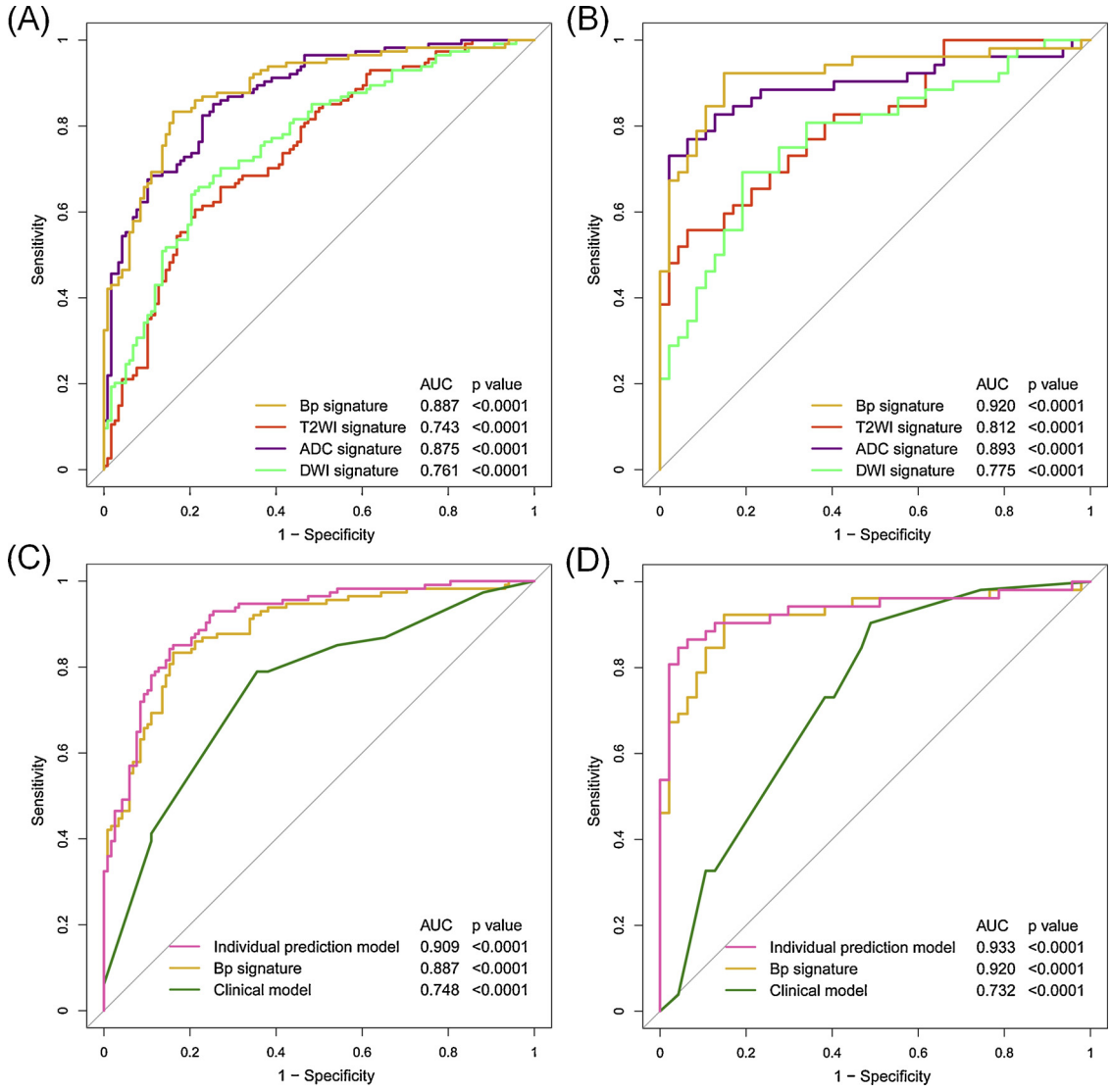

Fig. 2. The receiver operating curves of the four radiomics signatures in discriminating prostate cancer. (A) The primary cohort (B) The validation cohort. The efficiency of the three discrimination models is presented for (C) the primary cohort and (D) the validation cohort. The area under the receiver operating curve (AUC) is presented.

Table 3
Multivariable logistic regression analysis results.

Variable	Model 1			Model 2 (nomogram)		
	β	OR	P	β	OR	P
Intercept	−2.538		0.0001	−2.109		0.0005
Bp signature score	0.944	2.569 (2.011–3.282)	< 0.0001	0.931	2.536 (1.996–3.221)	< 0.0001
Age (2 vs. 1)	1.13	3.096 (0.963–9.950)	0.0578	1.256	3.513 (1.157–10.663)	0.0266
Age (3 vs. 1)	1.621	5.057 (1.416–18.066)	0.0126	1.654	5.228 (1.542–17.728)	0.0079
PSA (1 vs. 0)	1.382	3.982 (1.736–9.138)	0.0011	1.34	3.953 (1.731–8.945)	0.0011
CEA (1 vs. 0)	1.586	4.886 (0.556–42.916)	0.1525	NA	NA	NA
Hypertension (1 vs. 0)	0.794	2.212 (0.906–4.647)	0.0573	NA	NA	NA

incorporated three biochemical factors (i.e. the levels of CEA, CA 125, and CA 19-9), along with hypertension and diabetes, which were completely described in the patients' medical records. Univariate analysis showed that age, PSA level, and CEA level make sense in the discrimination of prostate cancer, which indicates that these three clinical factors were risk factors. Multivariable logistic regression analysis revealed that age and PSA level were independent clinical risk factors.

In several previous studies, the associations between DWI, ADC and prostate cancer have been proved [31,32]. T2W images are commonly applied to identify prostatic zonal anatomy, evaluate abnormalities within the prostate gland, and to assess invasive behavior. In our study, we found that none of the extracted features were associated with T2WI, which reflected that functional imaging provided more extra information about prostate cancer, compared to anatomical MR sequence.

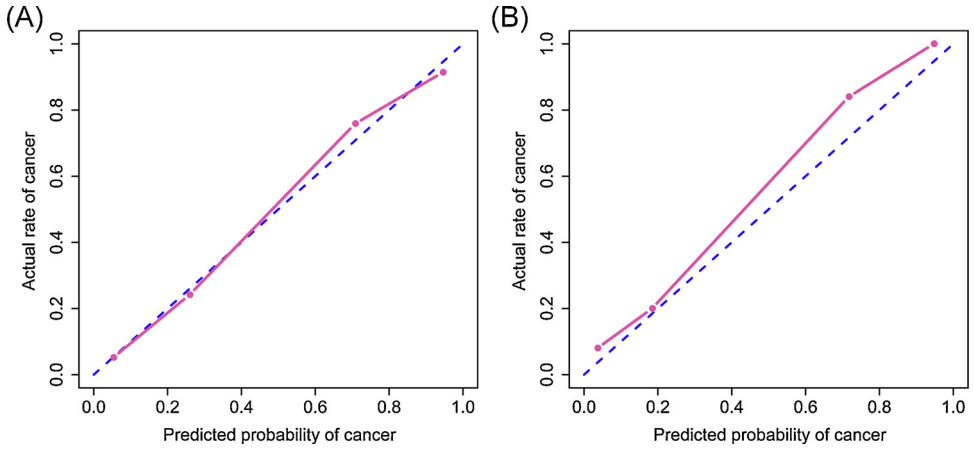

Fig. 3. Calibration curves of the developed individual prediction model. (A) The primary cohort. (B) The validation cohort.

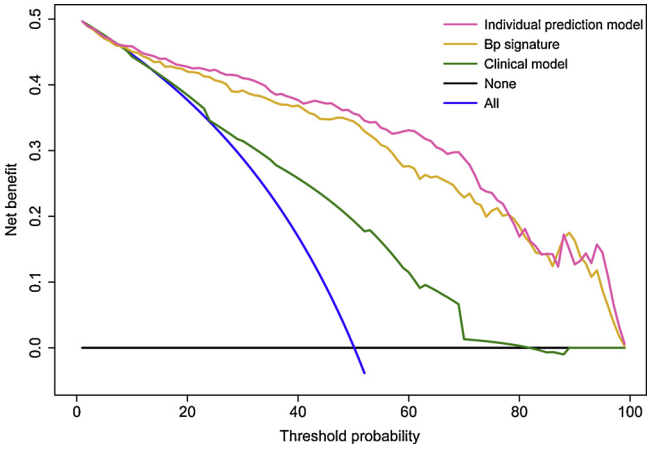

Fig. 4. Decision curve analysis for the three discrimination models.

We noted that, among the ultimately selected six features of bi-parametric MR images, one-half of these features were histogram-based features at different percentiles of the intensity of pixels in a region. Histogram analysis was used in previous tumor study, such as tumor discriminating and grading [33–35]. In this study, histogram analysis is part of the machine learning analysis applied to prostate cancer discrimination, we validated the role of traditional histogram feature in prostate cancer and other new machine learning features. Furthermore, to explore comprehensive information from images, we extracted multiple percentages of histogram feature from bp-MRI scans.

Aiming to investigate whether PZ and TZ can contribute to the discrimination of prostate cancer, we segmented lesions with cancer or with suspected cancer, as well as the PZ and TZ in the same section, which also was included in our inclusion criterion. Based on the results of our study, the features extracted from PZ and TZ had a more important role, even more so than the features extracted from the lesions.

Prior studies also used machine learning methods like texture analysis, fractal analysis to differentiating non-cancerous prostate from prostate cancer or detecting cancer [36,37]. Compared to these studies, our study had a relatively large number of experimental subjects and radiomics based on comprehensive machine learning methods. In addition, we combined clinical independent risk factors with Bp signature to build an individual prediction model.

Our study had some limitations. First, the radiomics analysis was retrospectively applied to existing single-center data, which needs further verification in a multicenter clinical study. Second, the segmentation results were manually conducted by radiology doctors. Third, in this study, we haven't compared our method with PI-RADS 2 guideline since lots of patients didn't have high b-value DWI images. In the future, the comparison with PI-RADS 2 should be investigated.

In providing the ability to mine imaging data, radiomics has broad application prospects in the fields of medical and individual diagnosis. Radiomics could be applied to solve various clinical problems, besides correlating imaging with pathological examination results. In further studies, we hope to correlate genomic characteristics and immunohistochemical information with radiomics to correlate with the Gleason score and aggressiveness of diagnosed prostate cancer and choose the most appropriate treatment programs with maximum therapeutic effect and minimum side effects.

In conclusion, firstly we investigated the bp-MRI based radiomics signature can serve as a predictive factor in prostate cancer discrimination. Secondly, we developed an individual prediction model incorporates Bp signature and the above clinical independent risk factors, which presents as an easy-to-use individual prediction model for doctors.

Conflict of interest

The authors of this manuscript declare no relationships with any companies, whose products or services may be related to the subject matter of the article.

Acknowledgements

We acknowledge financial support from the special program for science and technology development from the Ministry of science and technology, China, the Science and Technology Service Network Initiative of the Chinese Academy of Sciences, and National Natural Science Foundation of China.

Appendix A. Supplementary data

Supplementary material related to this article can be found, in the online version, at doi:https://doi.org/10.1016/j.ejrad.2019.02.032.

References

[1] R.L. Siegel, K.D. Miller, A. Jemal, Cancer statistics, 2016, CA Cancer J. Clin. 66 (2) (2016) 7–30.
[2] W. Chen, R. Zheng, P.D. Baade, et al., Cancer statistics in China, 2015, CA Cancer J. Clin. 66 (2) (2016) 115–132.
[3] N. Mottet, J. Bellmunt, M. Bolla, et al., EAU-ESTRO-SIOG guidelines on prostate cancer. Part 1: screening, diagnosis, and local treatment with curative intent, Eur. Urol. 71 (4) (2017) 618–629.
[4] F.H. Schröder, J. Hugosson, M.J. Roobol, et al., Screening and prostate-cancer mortality in a randomized European study, N. Engl. J. Med. 360 (13) (2009) 1320–1328.

[5] G.L. Andriole, E.D. Crawford, I.I.I.R.L. Grubb, et al., Mortality results from a randomized prostate-cancer screening trial, N. Engl. J. Med. 360 (13) (2009) 1310–1319.
[6] F.H. Schröder, J. Hugosson, M.J. Roobol, et al., Screening and prostate-cancer mortality in a randomized European study, N. Engl. J. Med. 360 (13) (2009) 1320–1328.
[7] D.J. Rosario, J.A. Lane, C. Metcalfe, et al., Short term outcomes of prostate biopsy in men tested for cancer by prostate specific antigen: prospective evaluation within ProtecT study, BMJ 344 (2012) d7894.
[8] H.A. Vargas, O. Akin, A. Afaq, et al., Magnetic resonance imaging for predicting prostate biopsy findings in patients considered for active surveillance of clinically low risk prostate cancer, J. Urol. 188 (5) (2012) 1732–1738.
[9] J.E. Thompson, D. Moses, R. Shnier, et al., Multiparametric magnetic resonance imaging guided diagnostic biopsy detects significant prostate cancer and could reduce unnecessary biopsies and over detection: a prospective study, J. Urol. 192 (1) (2014) 67–74.
[10] J.C. Weinreb, J.O. Barentsz, P.L. Choyke, et al., PI-RADS prostate imaging–reporting and data system: 2015, version 2, Eur. Urol. 69 (1) (2016) 16–40.
[11] H.A. Vargas, O. Akin, T. Franiel, et al., Diffusion-weighted endorectal MR imaging at 3 T for prostate cancer: tumor detection and assessment of aggressiveness, Radiology 259 (3) (2011) 775–784.
[12] M.A. Haider, T.H. Van Der Kwast, J. Tanguay, et al., Combined T2-weighted and diffusion-weighted MRI for localization of prostate cancer, Am. J. Roentgenol. 189 (2) (2007) 323–328.
[13] R.J. Gillies, P.E. Kinahan, H. Hricak, Radiomics: images are more than pictures, they are data, Radiology 278 (2) (2015) 563–577.
[14] Y. Huang, C. Liang, L. He, et al., Development and validation of a radiomics nomogram for preoperative prediction of lymph node metastasis in colorectal cancer, J. Clin. Oncol. 34 (18) (2016) 2157–2164.
[15] D. Dong, L. Tang, Z. Li, et al., Development and validation of an individualized nomogram to identify occult peritoneal metastasis in patients with advanced gastric cancer, Ann. Oncol. (2019) mdz001.
[16] J. Wu, T. Aguilera, D. Shultz, et al., Early-stage non–small cell lung Cancer: quantitative imaging characteristics of 18F fluorodeoxyglucose PET/CT allow prediction of distant metastasis, Radiology 281 (1) (2016) 270–278.
[17] B. Zhang, J. Tian, D. Dong, et al., Radiomics features of multiparametric MRI as novel prognostic factors in advanced nasopharyngeal carcinoma, Clin. Cancer Res. 23 (15) (2017) 4259–4269.
[18] L. Fan, M. Fang, Z. Li, et al., Radiomics signature: a biomarker for the preoperative discrimination of lung invasive adenocarcinoma manifesting as a ground-glass nodule, Eur. Radiol. 29 (2) (2019) 889–897.
[19] Y. R Liu, J. Kim, Y. Balagurunathan, et al., Radiomic features are associated with EGFR mutation status in lung adenocarcinomas, Clin. Lung Cancer 17 (5) (2016) 441–448 e6.
[20] S. Wang, J. Shi, Z. Ye, et al., Predicting EGFR mutation status in lung adenocarcinoma on CT image using deep learning, Eur. Respir. J. 0 (2019) 1800986.
[21] N.N. Tsiaparas, S. Golemati, I. Andreadis, et al., Comparison of multiresolution features for texture classification of carotid atherosclerosis from B-mode ultrasound, IEEE Trans. Inf. Technol. Biomed. 15 (1) (2011) 130–137.
[22] B. Turkbey, H. Mani, O. Aras, et al., Correlation of magnetic resonance imaging tumor volume with histopathology, J. Urol. 188 (2012) 1157–1163.
[23] M.B. Amin, D.W. Lin, J.L. Gore, et al., The critical role of the pathologist in determining eligibility for active surveillance as a management option in patients with prostate cancer: consensus statement with recommendations supported by the College of American Pathologists, International Society of Urological Pathology, Association of Directors of Anatomic and Surgical Pathology, the New Zealand Society of Pathologists, and the Prostate Cancer Foundation, Arch. Pathol. Lab. Med. 138 (2014) 1387–1405.
[24] L. Stamatakis, M.M. Siddiqui, J.W. Nix, et al., Accuracy of multiparametric magnetic resonance imaging in confirming eligibility for active surveillance for men with prostate cancer, Cancer 119 (2013) 3359–3366.
[25] Marina Mat Baki, Alex Menys, David Atkinson, Paul Bassett, Simon Morley, Timothy Beale, Guri Sandhu, et al., Feasibility of vocal fold abduction and adduction assessment using cine-MRI, Eur. Radiol. 27 (2) (2017) 598–606.
[26] J.P. Radtke, C. Schwab, M.B. Wolf, M.T. Freitag, C.D. Alt, C. Kesch, I.V. Popeneciu, C. Huettenbrink, C. Gasch, T. Klein, D. Bonekamp, Multiparametric magnetic resonance imaging (MRI) and MRI–transrectal ultrasound fusion biopsy for index tumor detection: correlation with radical prostatectomy specimen, Eur. Urol. 70 (5) (2016) 846–853.
[27] O. Reyes, C. Morell, S. Ventura, Scalable extensions of the ReliefF algorithm for weighting and selecting features on the multi-label learning context, Neurocomputing 161 (2015) 168–182.
[28] I.J. van Vlodrop, S.C. Joosten, T. De Meyer, K.M. Smits, L. Van Neste, V. Melotte, M.M. Baldewijns, L.J. Schouten, P.A. van den Brandt, J. Jeschke, J.M. Yi, A four-gene promoter methylation marker panel consisting of GREM1, NEURL, LAD1, and NEFH predicts survival of clear cell renal cell cancer patients, Clin. Cancer Res. 23 (8) (2017) 2006–2018.
[29] A.J. Vickers, E.B. Elkin, Decision curve analysis: a novel method for evaluating prediction models, Med. Decis. Making 26 (6) (2006) 565–574.
[30] J. Mohler, E. Antonorakis, A. Armstrong, NCCN Clinical Practice Guideline in Oncology. Prostate Cancer. Version 2.2017, (2017).
[31] T.H. Kim, J.Y. Jeong, S.W. Lee, et al., Diffusion-weighted magnetic resonance imaging for prediction of insignificant prostate cancer in potential candidates for active surveillance, Eur. Radiol. 25 (6) (2015) 1786–1792.
[32] Y. Peng, Y. Jiang, C. Yang, et al., Quantitative analysis of multiparametric prostate MR images: differentiation between prostate cancer and normal tissue and correlation with Gleason score—a computer-aided diagnosis development study, Radiology 267 (3) (2013) 787–796.
[33] O.F. Donati, Y. Mazaheri, A. Afaq, et al., Prostate cancer aggressiveness: assessment with whole-lesion histogram analysis of the apparent diffusion coefficient, Radiology 271 (1) (2013) 143–152.
[34] Y. Kang, S.H. Choi, Y.J. Kim, et al., Gliomas: histogram analysis of apparent diffusion coefficient maps with standard-or high-b-value diffusion-weighted MR imaging—correlation with tumor grade, Radiology 261 (3) (2011) 882–890.
[35] J.E. Park, H.S. Kim, K.J. Park, et al., Histogram analysis of amide proton transfer imaging to identify contrast-enhancing low-grade brain tumor that mimics high-grade tumor: increased accuracy of MR perfusion, Radiology 277 (1) (2015) 151–161.
[36] A. Wibmer, H. Hricak, T. Gondo, et al., Haralick texture analysis of prostate MRI: utility for differentiating non-cancerous prostate from prostate cancer and differentiating prostate cancers with different Gleason scores, Eur. Radiol. 25 (10) (2015) 2840–2850.
[37] D. Fehr, H. Veeraraghavan, A. Wibmer, et al., Automatic classification of prostate cancer Gleason scores from multiparametric magnetic resonance images, Proc. Natl. Acad. Sci. 112 (46) (2015) E6265–E6273.